Research Square

Preprints are preliminary reports that have not undergone peer review.
They should not be considered conclusive, used to inform clinical practice,
or referenced by the media as validated information.

Structural, Morphological, and Magnetic Properties of Ni–Zr Co- Substituted Cadmium Ferrite Nanoparticles Synthesized via Microwave- Assisted Sol–Gel Combustion

Pushpdas Gajbhiye

gajbhiye.pushpdas0@gmail.com

Rashtrasant Tukadoji Maharaj Nagpur University

Shilpa A. Pande

Laxminarayan Innovation Technological University

K. G. Rewatkar

Rashtrasant Tukadoji Maharaj Nagpur University

Research Article

Keywords: Spinel Ferrite NPs, Sol–Gel Combustion, Magnetic Properties, Cadmium Ferrite ($CdFe_2O_4$)

Posted Date: November 10th, 2026

DOI: https://doi.org/10.21203/rs.3.rs-11230268/v1

License: This work is licensed under a Creative Commons Attribution 4.0 International License.
Read Full License

Additional Declarations: No competing interests reported.

Structural, Morphological, and Magnetic Properties of Ni–Zr Co-Substituted Cadmium Ferrite Nanoparticles Synthesized via Microwave-Assisted Sol–Gel Combustion

Pushpdas B. Gajbhiye[1]*, Shilpa A. Pande[2]*, K. G. Rewatkar[3]

[1]Department of Physics, Rashtrasant Tukadoji Maharaj Nagpur University, Nagpur 440033, India

[2]Department of Applied Physics, Laxminarayan Innovation Technological University, Nagpur 440033, India

[3]Department of Physics, Vidya Vikas Arts, Commerce and Science College, Samudrapur 442305, India

*Corresponding Author | Email: gajbhiye.pushpdas0@gmail.com (PBG); sap7001@gmail.com (SAP)

ABSTRACT

Cadmium-based spinel ferrite nanoparticles with Ni and Zr co-substitution, having the target composition $CdFe_{2-x}(Ni, Zr)_{x/2}O_4$ (x = 0.0, 0.2, 0.4, 0.6, 0.8, and 1.0), were synthesized via a microwave-assisted sol–gel combustion technique. to investigate the combined influence of magnetic (Ni^{2+}) and non-magnetic (Zr^{4+}) cations on the structural and magnetic characteristics of $CdFe_2O_4$. The novelty of this work lies in systematically exploring the synergistic effect of simultaneous Ni–Zr co-substitution, which has received limited attention compared with individual cation substitution in cadmium ferrites. X-ray diffraction (XRD) analysis confirmed cubic spinel structures (space group $Fd\bar{3}m$) for initial composition. However, with the systematic increase in Ni-Zr substitution, appearance of secondary diffraction peaks of cubic CdO (space group Fm-3m). The average crystallite size progressively decreased from 29 nm (pure $CdFe_2O_4$) to 21 nm with increasing substitution, attributed to enhanced microstrain from the ionic size mismatch of Ni^{2+} and Zr^{4+}. The lattice constant decreased from 8.70 Å to 8.39 Å, consistent with Vegard's law. Williamson–Hall (W-H) plot analysis confirmed the strain-broadening effect. Scanning Electron Microscopy (SEM) micrographs revealed nearly spherical particle morphology with homogeneous grain distribution, while inter-particle agglomeration was observed due to high surface energy and magnetic interactions. Energy Dispersive X-ray (EDX) spectroscopy confirmed the presence of the intended constituent elements and a composition consistent with the nominal stoichiometry. Vibrating Sample Magnetometer (VSM) measurements at room temperature showed soft magnetic behavior for all compositions; saturation magnetization (Ms) peaked at 0.267 emu/g at x = 0.6 before declining at higher substitution levels, and coercivity (Hc) displayed a non-monotonic trend. The present results demonstrate that simultaneous Ni–Zr co-substitution provides an effective approach for tailoring the structural and magnetic properties of cadmium ferrite nanoparticles within the investigated composition range. These nanoparticles are promising candidates for soft magnetic and microwave absorption applications.

Keywords: Spinel Ferrite NPs; Sol–Gel Combustion; Magnetic Properties; Cadmium Ferrite ($CdFe_2O_4$)

1. INTRODUCTION

Magnetic spinel ferrites occupy a prominent place in the landscape of advanced functional materials owing to their remarkable structural versatility, tunable magnetic behavior, and broad applicability across scientific and industrial domains. The spinel ferrite structure, derived from the naturally occurring mineral magnesium aluminate ($MgAl_2O_4$), consists of a face-centered cubic (FCC) oxygen lattice hosting two distinct cation sublattices: tetrahedral (A) sites and octahedral (B) sites. These sites can accommodate a wide variety of divalent and trivalent metal cations, making it possible to engineer specific electrical, magnetic, and optical responses through careful compositional design. The general chemical formula of spinel ferrites is MFe_2O_4, where M is a divalent metal cation such as Mn, Mg, Zn, Ni, Co, Cu, or Cd, and Fe occupies the +3-oxidation state [1,2].

Interest in nanostructured spinel ferrites has grown substantially over the past two decades. At the nanoscale — typically below 100 nm — materials exhibit properties fundamentally different from their bulk counterparts, including a lower melting point, reduced sintering temperature, increased surface-to-volume ratio, enhanced chemical reactivity, and markedly altered magnetic characteristics such as superparamagnetism and modified coercivity [3,4]. These unique properties position nanocrystalline spinel ferrites at the forefront of research in medicine, catalysis, data storage, robotics, electromagnetic shielding, and microwave absorption [5,6].

Among various spinel ferrite families, cadmium ferrite ($CdFe_2O_4$) with a cubic spinel structure is an interesting base material, having high chemical stability, excellent saturation magnetization, and good magnetocrystalline anisotropy. Cadmium ferrite is a normal spinel where Cd^{2+} ions preferentially occupy the tetrahedral A-sites, and NiFe2O4 is a completely inverse spinel structure, due to Ni2+ has strong preference for the electrical conductivity octahedral B-site [7,8]. While pure cadmium ferrite exhibits a limited magnetic moment because of the non-magnetic nature of Cd^{2+}, its structural openness makes it highly receptive to ionic substitution. Substituting Fe^{3+} ions with transition metal or rare-earth cations is an effective strategy to enhance its magnetic, dielectric, and microwave properties [9,10].

M. Shkir et al.(2024) [7] were synthesized $CdFe_2O_4$ using Co-precipitation method and reported the effect of annealing temperature 700, 800, 900 °C on the structural, at room temperature magnetic, and optical properties. were crystallite size increases from 32 to 59nm with respect to the increasing temperature. Samples showed uniformly distributed highly agglomerated particles with larger voids surface morphology for samples annealed at 900 °C. The samples possess

ferromagnetic behavior, and the magnetization (Ms), Coercivity (Hc) 237.60 Oe, Retentivity (Mr) 1976×10−6 emu/g for the CdFe2O4 sample annealed at 900 °C. B. H. Devmunde et al. (2020) [8], have studied the structural, morphological, and infrared properties of $Ni_{1-x}Cd_xFe_2O_4$ (x=0.0, 0.1, 0.2, 0.3, 0.4, and 0.5) via the sol-gel auto-combustion method. They reported that for higher substitution of Cd^{2+} ions ($x \geq 0.5$), a secondary phase of Fe_3O_4 has been observed. The lattice constant is found to increase with increasing Cd^{2+} concentration. The particle size and average grain size from SEM were found to be in the range of 27-16 nm and 102-80 nm. R. Tiwari et al. [11] studied the structural, morphological, vibrational, and magnetic properties of pure and Cd- and Sr-ion-substituted nickel ferrite nanoparticles prepared by the self-ignited auto-combustion method and reported that cation substitution effectively modified the lattice parameter, cation distribution, vibrational characteristics, and magnetic properties. P. Murthy et al. [12] demonstrated Nd^{3+} substituted Ni-Cd ferrites using a novel solution combustion method; they predicted an increase in lattice parameter with an increase in Cd^{2+} ion content. The room-temperature Ms, Mr, Hc increases attain maximum and thereafter decrease with increasing Cd^{2+} and Nd^{3+} ions. R. Pathare et al. [13] have recently studied the impact of La^{3+} and Dy^{3+} ion substitution in cadmium ferrite. Large ionic radius ions significantly altered structural and magnetic properties. R. Rajenimbalkar et al. [14] reported that Ti^{4+}–Zn^{2+} co-doping in the $NiFe_2O_4$ spinel lattice significantly influenced the structural and magnetic properties through lattice distortion and cation substitution. These findings suggest that multi-cation co-doping is a promising approach for tailoring spinel ferrites. M. Satish et al. (2023) [15] have studied the effect of Zr4+ on octahedral sites using $NiFe_{1.8}Zr_{0.2}O_4$ tartrate-gel method, and reported that a small impurity (ZrO2) was observed in the NiFe1.8Zr0.2O4 sample, as well as a mean crystal size 11nm (without Zr) and 8 nm (with Zr substitution), Ms and Hc decreases from 48-41 and 84-97 while substituting Zr. R. El-Shater et al. [16] reported that the Zr^{4+} substituted Ni-Zn ferrites significantly influenced the structural, magnetic, and dielectric properties. A mixed phase appears at higher concentrations of Zr^{4+} as a result of modification in lattice parameter and cation distribution S. Wanjari et al. [17] reported that the reason for the formation of a secondary phase and limited solubility of "La^{3+} ions in the spinel lattice. H. Nazli et al.(2026) [18] prepared a $CdFe_2O_4$ thin film using the electrodeposition method for oxidation times ranging from 10 to 30 min to investigate the influence of oxidation time on their properties and studied the structural, magnetic, and electrical properties, and reported that crystallite size ranged from 21.07 to 45.01 nm. They reported interconnected cuboidal and polyhedral grains averaging 147.25 nm, a maximum saturation magnetization of 30.27 emu/cm³, and a coercivity of 654.28 Oe. C.G. Singh et al. (2025) [19] synthesized zinc Cobalt-Zirconyl ferrite nanoparticles using

sol-gel auto-combustion and reported Ms. (1.807 to 1.279 emu/g), low Mr. (0.39 to 0.22 emu/g), and Hc (0.086 to 0.043 Oe) values.

SP. Keerthana et al. (2024) [20] synthesized $CdFe_2O_4$, 1 % Gd-$CdFe_2O_4$, 2 % Gd-$CdFe_2O_4$ using hydrothermal route and reported that the pure Cd ferrite has octahedron like morphology while1 1%,2% Gd doped has octahedron and rod. A. Nandanwar et al. (2017) [21] Ni substituted Cd ferrite were produced using Sol-gel micro-oven method and reported that the formation of monophasic powder with average particle size 5.55-5.50 nm. K. Harish et al. (2026) [22] prepared $CdFe_2O_4$ and Zr-$CdFe_2O_4$ using a facile green-mediated *(Tulasi extract)* combustion method. They reported that the XRD results show a particle size of 21 nm and a spinel-structured crystalline nature.

N Mohammed et al. (2025) [23] examined $Ni_{0.65}Cd_{0.35}Fe_{2-x}Al_xO_4$ ($0 \leq x \leq 0.060$) **S**ingle-phase spinel structure via sol–gel method and found the Crystalline size (40–36) nm, Ms 62.78- 61.60, and Hc 40.19 - 46.08, with decreasing grain size with increasing Al content. A. Teber et al. (2023) [24] studied the effect of zirconium (Zr) substitution in nickel–cobalt ferrites produced by the hydrothermal method and demonstrated the results for electrical, magnetic, and microstructural characteristic properties. they detect M type hexagonal and tetragonal nanocrystallites of 32 and 67 nm with a tetragonal ZrO2 secondary phase as well as low saturation magnetization ranging from 0.127-0.101 emu/g. K. Langade et al. (2025) [25] prepare $Ni_{0.5}Cd_{0.5}Fe_{2-x}Cr_xO_4$) via the sol-gel auto-combustion method and reported the Ms value 0..42-0.15emu/g.

According to the literature report and the above discussion, most work has focused on pure Cd ferrite or Ni ferrite and other metal ion-doped spinel ferrites. Very little work has been reported on Cd-based spinel ferrites. Such as Rare-earth metal ion Dy^{3+} [13], La^{3+} [17] (non-magnetic); transition metal ion Ti4+ [14], Zr^{4+} [16] (non-magnetic), having a large ionic radius compared with Cd, their incorporation into the spinel ferrite lattice altered the crystal structure, cation distribution, and magnetic properties. This suggests that appropriate cation substitution is an effective strategy for tailoring the functional properties of $CdFe_2O_4$, motivating the present study to investigate the influence of simultaneous Ni^{2+}–Zr^{4+} co-substitution.

Nickel (Ni^{2+}) and zirconium (Zr^{4+}) are particularly interesting dopants for this purpose. Nickel ferrite ($NiFe_2O_4$) is an inverse spinel with well-known soft magnetic characteristics including high permeability, high resistivity, and high saturation magnetization [3,26]. Zirconium, being a non-magnetic tetravalent ion, alters the cation distribution and influences super exchange interactions when substituted into the spinel lattice. Prior studies on Zr-doped cobalt ferrites

have demonstrated that Zr^{4+} substitution reduces crystallite size and modifies magnetic anisotropy due to the ionic radii mismatch between Zr^{4+} (0.72 Å) and Fe^{3+} (0.645 Å) [27]. Complementary work from our research group on Al, Ni–Cd, and Cu–Ni ferrites synthesized by microwave-assisted combustion has further established the sensitivity of structural and magnetic properties to cation substitution [28,29,30].

The microwave-assisted sol–gel combustion technique offers several notable advantages over conventional sintering, including rapid processing, better homogeneity, finer particle size, and excellent compositional control [31,32,33]. The present work systematically investigates how the progressive replacement of Fe^{3+} by equal parts Ni^{2+} and Zr^{4+} affects the crystal structure, grain morphology, elemental composition, and magnetic behaviour of $CdFe_{2-x}(Ni, Zr)_{x/2}O_4$ nanoparticles.

2. SYNTHESIS AND METHODOLOGY

2.1 Materials

All chemicals used in this study were of analytical reagent grade and were used as received without further purification. The following precursors were employed: Ferric Nitrate Nonahydrate [$Fe(NO_3)_3 \cdot 9H_2O$, ≥98%, SRL], Cadmium Nitrate Tetrahydrate [$Cd(NO_3)_2 \cdot 4H_2O$, ≥99%, SRL], Nickel(II) Nitrate Hexahydrate [$Ni(NO_3)_2 \cdot 6H_2O$, ≥99%, SRL], Zirconyl Nitrate Hydrate [$ZrO(NO_3)_2 \cdot xH_2O$, ≥99.5%, SRL], and Urea [CH_4N_2O, ≥99.5%, SRL] as the fuel and complexing agent. Stoichiometric quantities of each precursor were calculated based on the desired composition $CdFe_{2-x}(Ni, Zr)_{x/2}O_4$ for x = 0.0, 0.2, 0.4, 0.6, 0.8, and 1.0, While Cadmium content was maintained at a constant molar ratio of 1 throughout all compositions.

2.2 Synthesis of Ni–Zr Co-substituted $CdFe_2O_4$ Nanoparticles

The ferrite nanoparticles were synthesized using a microwave-assisted sol–gel auto-combustion method because of its ability to produce chemically homogeneous nanocrystalline ferrites within a short reaction time while minimizing energy consumption.

Initially, stoichiometric amounts of cadmium nitrate, ferric nitrate, nickel nitrate, zirconyl nitrate, and urea were dissolved separately in approximately 50 mL of deionized water in a 100 mL beaker and subsequently mixed under continuous magnetic stirring. Urea served both as a complexing agent and combustion fuel, promoting homogeneous mixing of the constituent metal ions and facilitating the subsequent self-propagating combustion reaction. The mixed precursor solution was heated on a magnetic hot plate at **80–100 °C** until a highly viscous sol was formed, which gradually transformed into a homogeneous gel. The obtained gel was immediately transferred into a domestic microwave oven operating at **700 W**, where rapid microwave irradiation initiated a self-sustained combustion reaction. The combustion process was

completed within approximately **2–3 min**, producing a voluminous, porous brown-black precursor powder.

The combustion product was allowed to cool naturally to room temperature before being finely ground using an agate mortar for approximately **2 h** to improve powder homogeneity. The ground powder was subsequently calcined in air at **800 °C for 6 h** in a programmable muffle furnace to improve crystallinity and promote the formation of the spinel ferrite phase. After calcination, the powders were reground for an additional **2 h** to obtain uniformly dispersed nanocrystalline ferrite powders suitable for structural, morphological, and magnetic characterization.

2.3 Structural Characterization

The crystal structure and phase evolution of the synthesized samples were investigated using a Rigaku MiniFlex 600 X-ray diffractometer equipped with Cu-Kα radiation (λ=1.5406\lambda = 1.5406λ=1.5406 Å), operated at 40 kV and 15 mA. Diffraction patterns were collected over the 2θ range of 20–80° using a scan step of 0.02°.

The average crystallite size was estimated using the Debye–Scherrer equation

$$\mathbf{D = K\lambda / \beta\cos\theta}$$

where **D** is the crystallite size, **K = 0.9** is the shape factor, **λ** is the X-ray wavelength, **β** is the full width at half maximum (FWHM) expressed in radians, and **θ** is the Bragg diffraction angle. [37]

The lattice parameter of the cubic spinel phase was calculated using

$$\boldsymbol{a = d\sqrt{h^2 + k^2 + l^2}}$$

where d represents the interplanar spacing corresponding to the indexed diffraction plane.[12]

To evaluate the simultaneous contribution of crystallite size and lattice strain to peak broadening, Williamson–Hall (W–H) analysis was performed according to

$$\mathbf{\beta\cos\theta = K\lambda / D + 4\varepsilon\sin\theta}$$

where,

D represents the crystallite size and **ε** denotes the lattice microstrain.

The crystallite size and lattice strain were obtained from the intercept and slope of the linear Williamson–Hall plots, respectively.[35]

2.4 Morphological and Elemental Characterization

The particle morphology and surface microstructure were examined using a JEOL JSM-6390LA scanning electron microscope (SEM) operating at an accelerating voltage of 20 kV.

Elemental composition was investigated using an Oxford Instruments XMX-N Energy Dispersive X-ray Spectroscopy (EDX) system attached to the SEM.

The elemental analysis was employed to verify the presence of Cd, Fe, Ni, Zr, and O in the synthesized samples and to compare the experimentally measured elemental ratios with the nominal stoichiometric compositions. Since EDX is a compositional analysis technique rather than a crystallographic technique, it was used only to confirm elemental composition and compositional uniformity.

2.5 Magnetic Characterization

Room-temperature magnetic measurements were carried out using a Lake Shore Model 7407 Vibrating Sample Magnetometer (VSM) under an applied magnetic field of ±20 kOe. The magnetic hysteresis (M–H) loops were analyzed to determine the principal magnetic parameters, including saturation magnetization (Ms), remanent magnetization (Mr), coercivity (Hc), squareness ratio (Mr/Ms), magnetic moment, and magnetocrystalline anisotropy constant. The squareness ratio was calculated using $R = M_r / M_s$ [12]

while the effective anisotropy constant was estimated using

$$\mathbf{K = (Hc \cdot M_s) / 0.96}$$

Where **Hc** is expressed in Oe and $\mathbf{M_S}$ in emu g^{-1}.

2.6 Data Analysis and Statistical Treatment

All diffraction data were indexed using standard ICDD reference files for cubic spinel $CdFe_2O_4$. Peak positions, FWHM values, and lattice parameters were obtained through least-squares fitting. Williamson–Hall plots were analysed using linear regression to estimate crystallite size and lattice strain.

SEM micrographs were qualitatively examined to evaluate particle morphology and agglomeration. The EDX spectra were analysed by comparing the measured elemental composition with the theoretical stoichiometric ratios corresponding to each nominal composition.

Magnetic parameters were extracted directly from the experimentally measured hysteresis loops. All magnetic calculations, including squareness ratio and anisotropy constant, were recalculated and verified to ensure internal consistency before interpretation.

3. RESULTS AND DISCUSSION

3.1 Structural Analysis: X-ray Diffraction (XRD)

The XRD patterns of $CdFe_{2-x}(Ni, Zr)_{x/2}O_4$ nanoparticles for all compositions are shown in Figure 1. The pure sample (x = 0.0) matches precisely with ICDD standard file No. 00-022-1063 for cadmium ferrite, confirming a phase-pure cubic spinel structure. Characteristic diffraction peaks corresponding to planes (220), (311), (222), (400), (331), (422), (511), (440), (620), (533),

(622), and (511) are observed in the 2θ range 20°–80°, consistent with space group $Fd\bar{3}m$ [6,42]. With increasing Ni–Zr substitution, all peaks shift systematically to higher 2θ angles, reflecting a contraction of the unit cell. The lattice constant decreases from 8.70 Å (pure) to 8.39 Å (x = 1.0), summarized in Table 1. As the substitution level increases, the excess CdO (Fm-3m) phase peaks start to emerge due to the limited solubility of the larger Zr^{4+} ion (0.72 Å) in the spinel lattice [27,43].

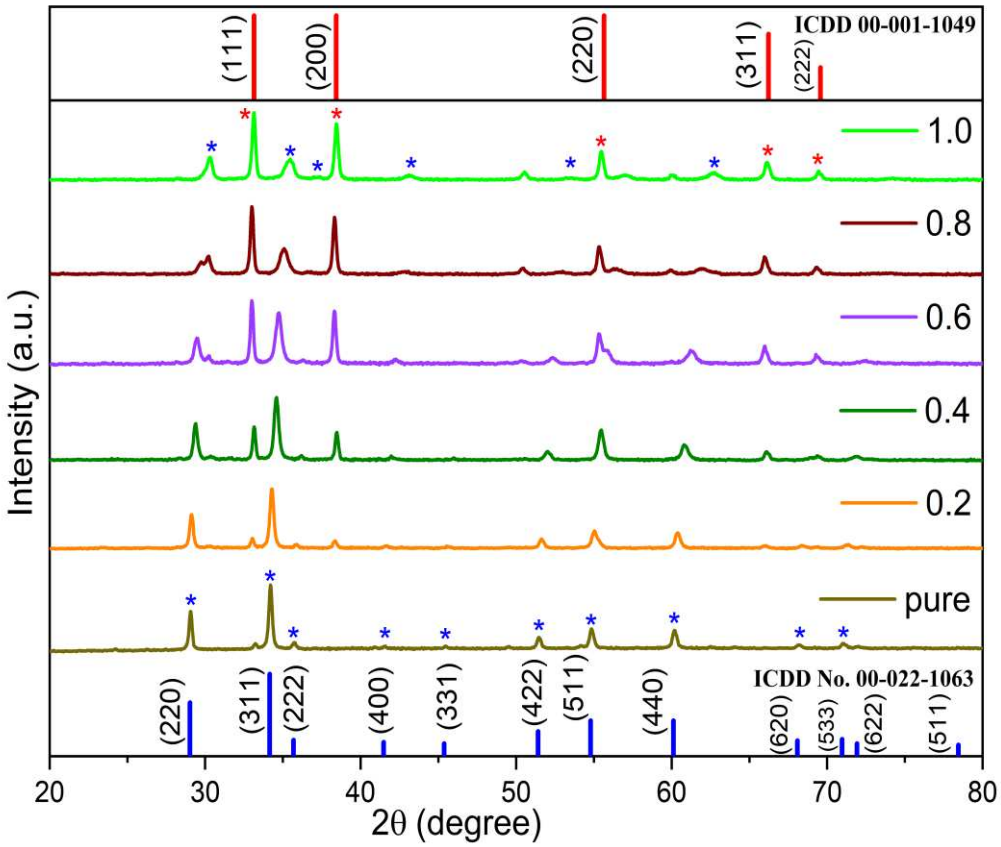


Figure 1: X-ray diffraction patterns of $CdFe_{2-x}(Ni, Zr)_{x/2}O_4$ (x = 0.0, 0.2, 0.4, 0.6, 0.8, 1.0) nanoferrite powder samples. Blue asterisk (*) indicates cubic phase of fd-3m space group, and red asterisk (*) indicates cubic phase of CdO of fm-3m space group

The (311) reflection — the most intense peak of the spinel structure — broadens with increasing substitution is agrees with previously reported studies where a reduction in crystal size and an increase in microstrain [11,36] are observed, indicating a reduction in crystallite size. Crystallite size D, calculated from the (311) peak using the Debye–Scherrer equation $D = k\lambda/\beta\cos\theta$, decreases from 38.83 nm (pure) to 12.91 nm (x = 1.0). The average crystallite size computed from all peaks decreases from 29 nm to 21 nm. This progressive reduction is a direct consequence of enhanced microstrain resulting from the ionic size mismatch of the substituting cations, which impedes grain growth during calcination [27,44]

Figure 2 presents the Williamson–Hall (W-H) plots for all compositions. The slope of each linear fit is proportional to the microstrain present in the sample, while the y-intercept yields the crystallite size. The increasing slope with Ni–Zr content confirms that lattice strain progressively increases with substitution [31,28].

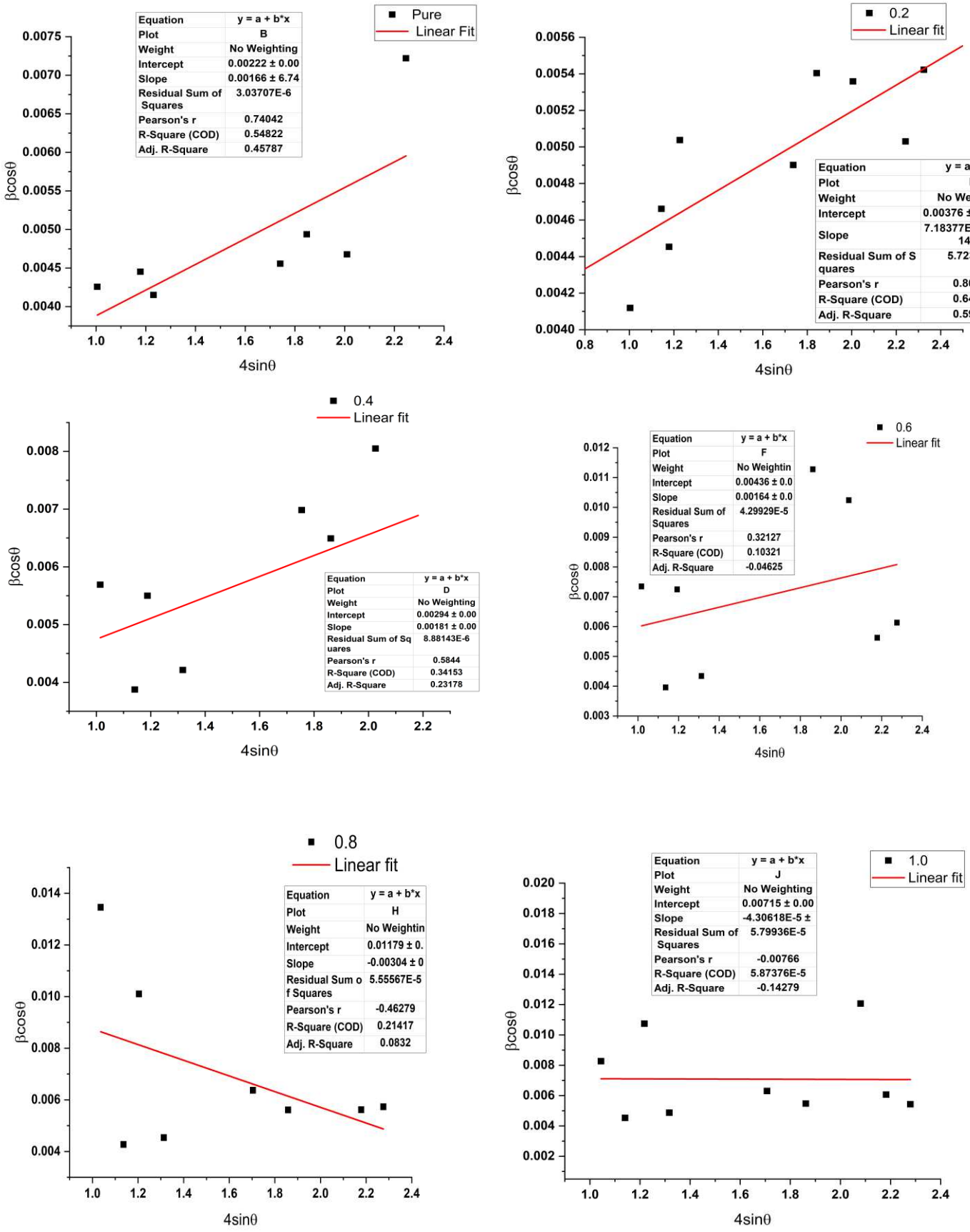


Figure 2: Williamson–Hall (W-H) plots for $CdFe_{2-x}(Ni, Zr)_{x/2}O_4$ at x = Pure, 0.2, 0.4, 0.6, 0.8, and 1.0. The slope of the linear fit is proportional to microstrain; increasing slopes with substitution confirm enhanced lattice strain.

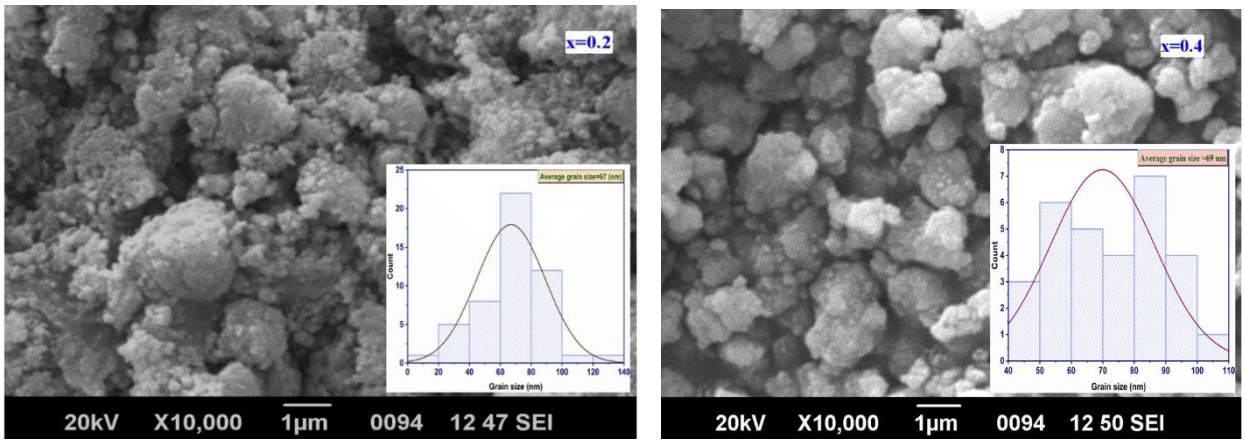
Table 1: Results of XRD Analysis for $CdFe_{2-x}(Ni, Zr)_{x/2}O_4$ (x = 0.0–1.0)

Sr.No.	x	2θ (311)°	d (Å)	a (Å)	a^3 (Å^3)	D (nm)	ρx (g/cm^3)	Avg D (nm)	D from W-H (nm)
1	Pure	34.15	2.62	8.70	658.5	38.83	23.81	29	62
2	0.2	34.27	2.61	8.66	649.46	31.13	23.55	28	36
3	0.4	34.55	2.59	8.60	636.05	25.21	23.45	25	47
4	0.6	34.71	2.58	8.57	629.45	19.93	23.10	22	31
5	0.8	35.03	2.55	8.48	609.80	13.72	23.24	22	10
6	1.0	35.45	2.53	8.39	590.58	12.91	23.34	21	19

3.2 Surface Morphology: Scanning Electron Microscopy (SEM)

The SEM micrographs with histogram of $CdFe_{2-x}(Ni, Zr)_{x/2}O_4$ nanoparticles for x = 0.2 to 1.0 are shown in Figure 3. All samples exhibit predominantly nearly spherical particle morphology with a reasonably homogeneous spatial distribution. The nearly spherical shape is a characteristic outcome of the rapid, self-sustaining exothermic sol–gel combustion reaction, which limits anisotropic growth [45,46].

Significant particle agglomeration is observed across all compositions. This arises from the high surface energy of nanoparticles with very large surface-to-volume ratios, which drives surface energy minimization through inter-particle contact, and from strong magnetic dipole–dipole interactions between nanoparticles [45,37]. The degree of visible agglomeration appears to increase in samples with higher substitution levels, consistent with the smaller crystallite sizes confirmed by XRD. Histogram shows average grain size, in the range of 67 to 98 nm as shown in table 2.



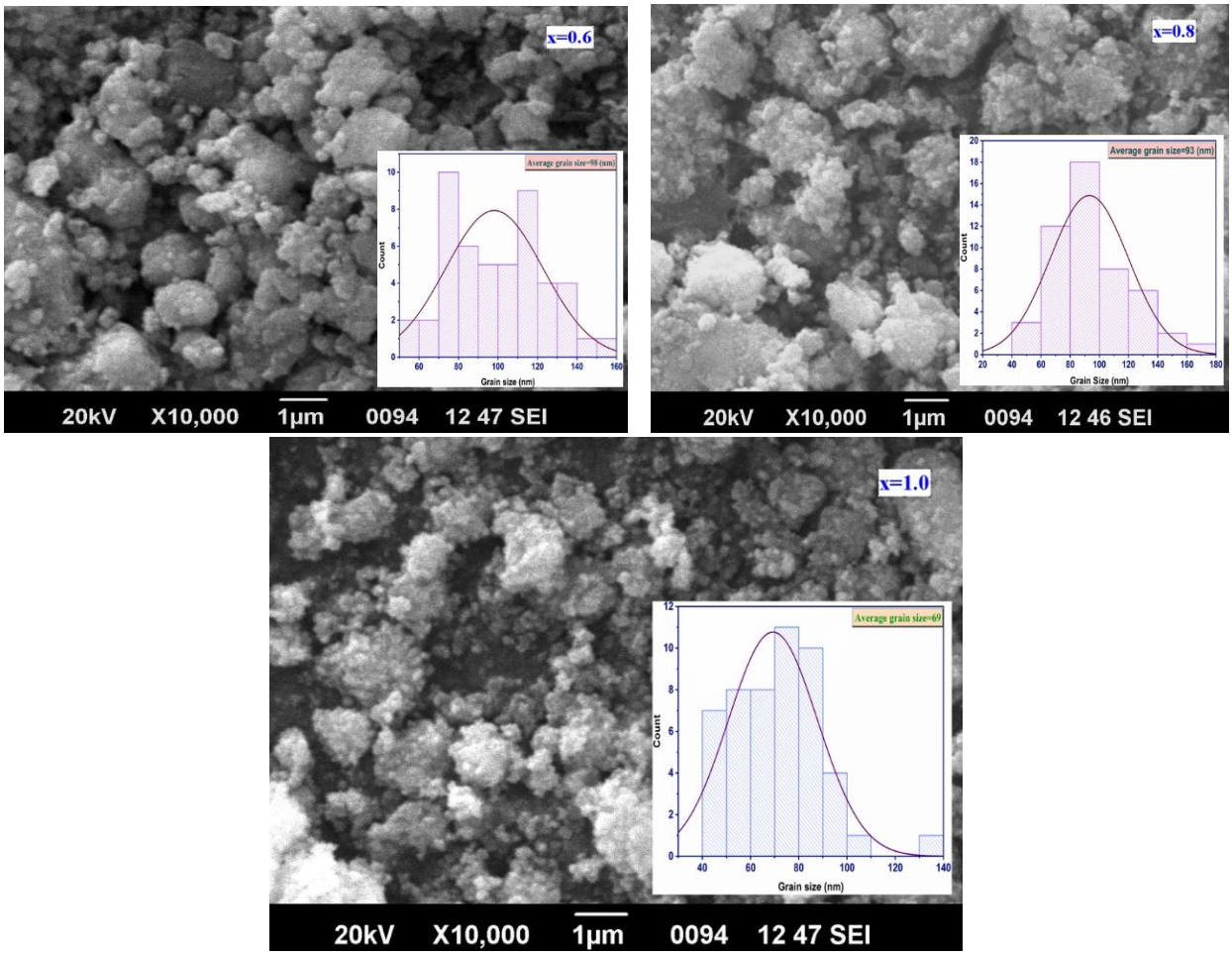


Figure 3: SEM micrographs with histogram of $CdFe_{2-x}(Ni, Zr)_{x/2}O_4$ nanoparticles at x = 0.2, 0.4, 0.6, 0.8, and 1.0 (×10,000 magnification, 20 kV), showing nearly spherical grain morphology and agglomeration due to magnetic inter-particle interactions.

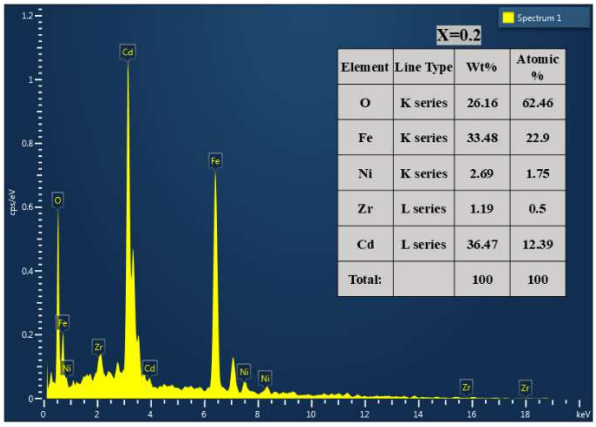
Table 2: average grain size and standard deviation extracted from SEM micrographs

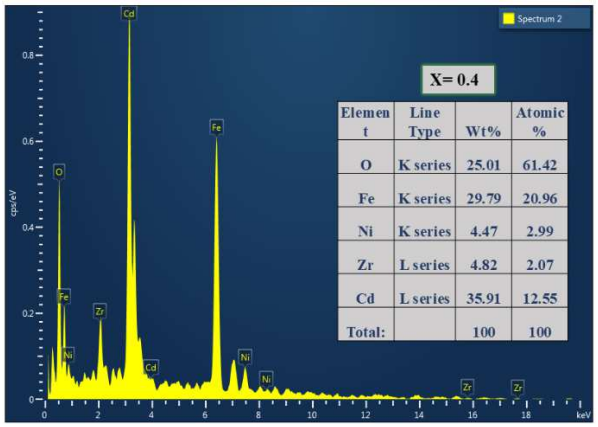
Sr. No.	Substitution (x)	Average Grain size (nm)	Standard Deviation (nm)
1	0.2	67	22
2	0.4	69	17
3	0.6	98	25
4	0.8	93	27
5	1.0	69	19

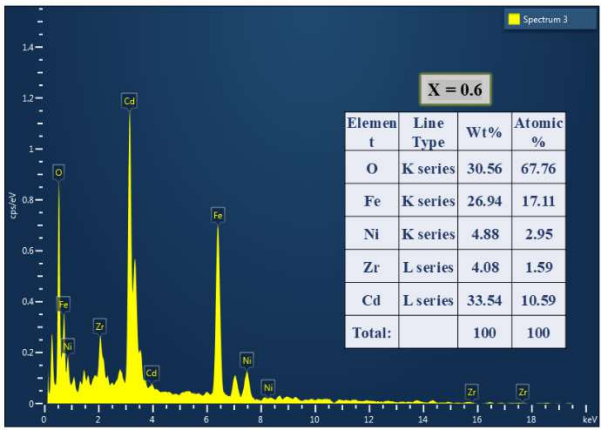
Crystallite size calculated using Debye–Scherrer equation goes decreases with increasing substitution of Ni-Zr and average grain size calculated from histogram shown in the table 2 does not show systematic variation ranging from 67-98 nm. The larger grain size compares with the crystallite size suggest that the observed grain may consist of agglomeration of several nanocrystalline, crystal size reduction increases relative surface atom contribution which can cause surface spin disorder as well as spin canting, thereby contribution to reduction of Ms inside grain increases results in increasing surface to volume ratio.[25]

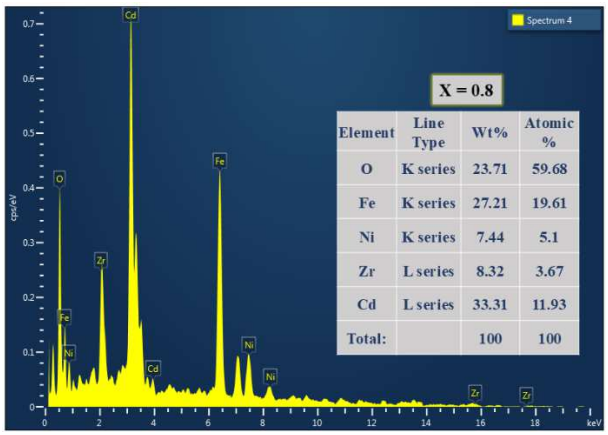
3.3 Elemental Analysis: Energy Dispersive X-ray (EDX) Spectroscopy

Energy Dispersive X-ray (EDX) spectra were recorded for all samples to confirm elemental composition (Figure 4). The spectra show characteristic emission lines for oxygen (O, K series), iron (Fe, K series), cadmium (Cd, L series), nickel (Ni, K series), and zirconium (Zr, L series). No additional elemental peaks attributable to foreign elements are detected in any spectrum [42,43]. As substitution level x increases, the weight and atomic percentages of Ni and Zr progressively increase while those of Fe correspondingly decrease, in full agreement with the intended substitution chemistry.









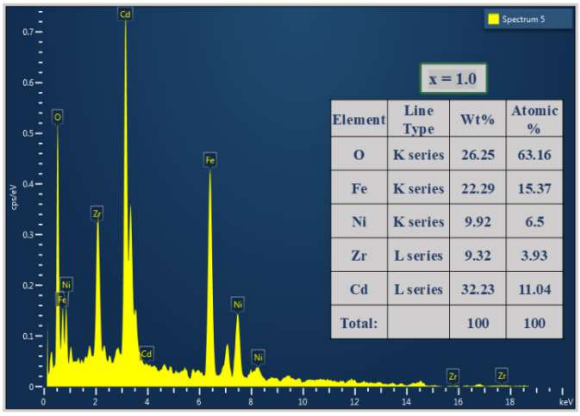


Figure 4: EDX spectra of $CdFe_{2-x}(Ni, Zr)_{x/2}O_4$ ferrite nanoparticles at x = 0.2, 0.4, 0.6, 0.8, and 1.0, confirming the presence of Fe, Cd, Ni, Zr, and O with no foreign elemental impurities. Table inside figure shows observed experimentally atomic weight and atomic percentage.

Table 3: shows theoretical element composition of weight percentage and atomic percentage

Element	0.2		0.4		0.6		0.8		1.0	
	Wt%	At%	Wt%	At%	Wt%	At%	Wt%	At%	Wt%	At%
Cd	38.505	14.28	38.0081	14.28	37.5234	14.28	37.0508	14.28	36.5021	14.28
Fe	34.436	25.71	30.2145	22.85	26.1004	20	22.09	17.14	18.1794	14.28
Ni	2.0104	1.42	3.9688	2.85	5.8773	4.28	7.7377	5.71	9.5519	7.14
Zr	3.1247	1.42	6.1686	2.85	9.1350	4.28	12.0266	5.71	14.8462	7.14
O	21.9229	57.14	21.6397	57.14	21.3637	57.14	21.0946	57.14	20.8323	57.14

3.4 Magnetic Properties: VSM Analysis

Room-temperature M-H hysteresis loops of $CdFe_{2-x}(Ni, Zr)_{x/2}O_4$ nanoparticles for x = 0.0 to 1.0 are shown in Figure 5. All samples display the characteristic S-shaped hysteresis loop typical of soft magnetic materials, with narrow loop widths and low coercive fields. The S-type behavior and near-zero remanence at low fields well-controlled magnetic anisotropy [29,30].

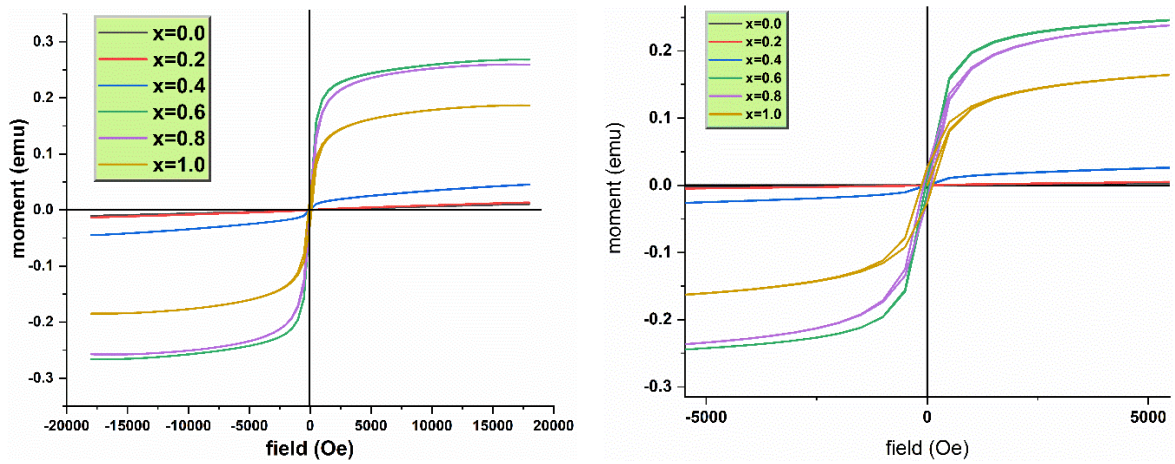


Figure 5: M-H hysteresis loops of $CdFe_{2-x}(Ni, Zr)_{x/2}O_4$ nanoparticles (x = 0.0–1.0) showing (left) full field range ±20,000 Oe and (right) expanded view at ±1,500 Oe, confirming soft magnetic behavior for all compositions.

The saturation magnetization (Ms) exhibits a non-monotonic trend with increasing substitution. Starting at 0.0103 emu/g for pure $CdFe_2O_4$, Ms increases substantially to a peak of 0.267 emu/g at x = 0.6, before declining to 0.185 emu/g at x = 1.0. The low Ms of pure cadmium ferrite reflects the non-magnetic nature of Cd^{2+}, which disrupts the antiparallel superexchange interactions between sublattices. Introduction of Ni^{2+} (magnetic moment 2μB) at B sites progressively strengthens the B-sublattice moment [3,44]. Beyond x = 0.6, the non-magnetic Zr^{4+} ions dilute the B-sublattice magnetic moment, causing Ms to decline [27,43]. Coercivity (Hc) decreases sharply from 278.85 Oe (pure) to a minimum of 22.03 Oe at x = 0.4, then increases to 125.36 Oe at x = 1.0, reflecting competing effects of reduced magnetic anisotropy from Ni^{2+} and increased structural strain from Zr^{4+} [27,44,45]. The squareness ratio (R = Mr/Ms) is below 0.5 for most compositions, indicating a multi-domain particle structure [46].

The relatively low saturation magnetization observed in the present study, the Ni-Zr co-substitution in cadmium ferrite nanoparticles attributed to the combine effects of magnetic dilution, increasing lattice strain, lattice distortion, cation redistribution, evolution of secondary phase with increasing substitution of non-magnetic Zr^4 ions has large ionic radius (0.72Å). Similar suppression, and non-monotonic variation of saturation magnetization with increasing Zr substitution in Co-Ni ferrite nanostructure observed by A teber et al. [24]. Increase in lattice strain calculated from W-H plot and nanoscale nature of the particle increases surface-to-volume ratio that increases the fraction of surface. Broken exchange bond and structural disorder results in long range spin alignment canted or disordered the surface spin and contribute to the effectively lees net magnetization. Similar suppression shown in recent study on Cr substituted Ni-Cd ferrite nanoparticles where the unusual low Ms = 0.15 emu/g [25]

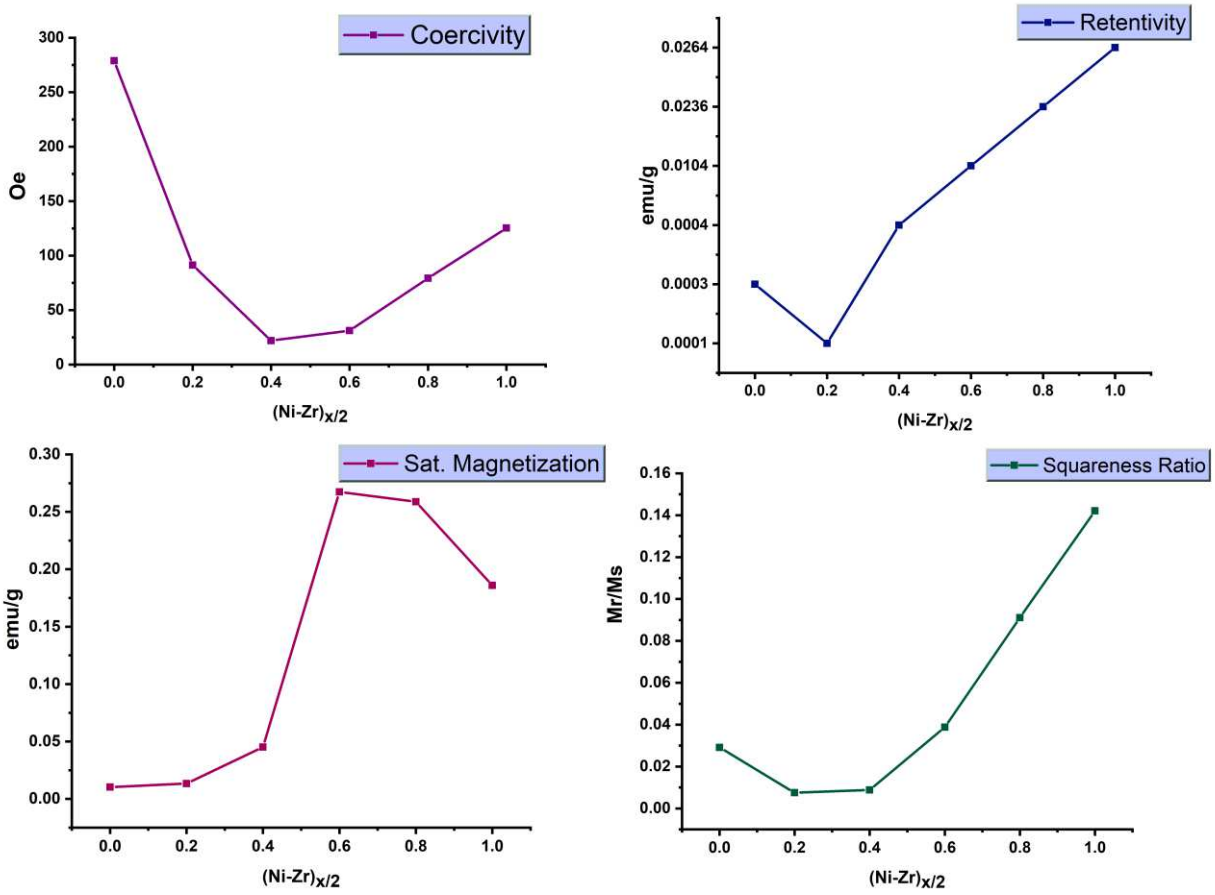


Figure 6: Graphical representation of the variation of coercivity, retentivity, saturation magnetization, and squareness ratio as a function of Ni–Zr substitution (x = 0.0–1.0) in $CdFe_{2-x}(Ni, Zr)_{x/2}O_4$ nanoparticles.

Table 4: VSM Magnetic Parameters for $CdFe_{2-x}(Ni, Zr)_{x/2}O_4$ (x = 0.0–1.0)

Parameter	x=0 (Pure)	x=0.2	x=0.4	x=0.6	x=0.8	x=1.0
Coercivity	278.85	91.371	22.026	31.241	79.223	125.359
Sat. Magnetization	0.0103	0.0133	0.0451	0.2674	0.2588	0.1859
Retentivity	3.385e−4	1.423e−4	4.836e−4	1.044e−2	0.0236	2.647e−2
Squareness Ratio	0.0291	0.0075	0.0088	0.0388	0.0911	0.1421
Bohr Magneton	0.0021	0.0027	0.1	0.0523	0.049	0.0343
Anisotropy Const.	2.991	1.265	1.0324	8.689	21.291	24.157

4. CONCLUSION

This study successfully demonstrated the synthesis of $CdFe_{2-x}(Ni, Zr)_{x/2}O_4$ nanoparticles (x = 0.0–1.0) using a simple, rapid, and cost-effective microwave-assisted sol–gel combustion technique. XRD analysis confirmed single-phase cubic spinel structures ($Fd\bar{3}m$) initially and gradually forming a secondary phase of CdO for higher compositions, with the lattice constant decreasing from 8.70 Å to 8.39 Å and crystallite size reducing from 29 nm to 21 nm with

increasing substitution. Williamson–Hall plot analysis confirmed the dominant role of lattice strain in peak broadening. SEM analysis revealed nearly spherical particle morphology with homogeneous grain distribution; agglomeration arising from inter-particle magnetic interactions was consistently observed across all compositions. EDX spectroscopy confirmed the compositional purity of each sample with no foreign elemental contamination.

VSM measurements demonstrated soft magnetic behavior for all compositions. Saturation magnetization peaked at x = 0.6 (Ms = 0.267 emu/g), consistent with finding report by A. Teber et al [24] and K. Langade et al [25] driven by strengthened B-sublattice magnetic moment from Ni^{2+} incorporation, before declining at higher Zr^{4+} concentrations due to non-magnetic dilution. Coercivity exhibited a non-monotonic trend governed by competing anisotropy contributions. The results collectively demonstrate that the structural and magnetic properties of cadmium ferrite nanoparticles can be systematically tuned through Ni–Zr co-substitution. The composition range x = 0.4–0.6 offers a particularly promising combination of elevated saturation magnetization and low coercivity, making these materials attractive candidates for soft magnetic devices and electromagnetic wave absorption applications.

REFERENCES

[1] Vinnik, D.A., et al. (2022). Impact of the Zn–Co content on structural and magnetic characteristics of the Ni spinel ferrites. Ceramics International, 48(13), 18124–18133.

[2] Amiri, M., Salavati-Niasari, M., & Akbari, A. (2019). Magnetic nanocarriers: evolution of spinel ferrites for medical applications. Advances in Colloid and Interface Science, 265, 29–44.

[3] Narang, S.B., & Pubby, K. (2021). Nickel spinel ferrites: a review. Journal of Magnetism and Magnetic Materials, 519, 167163.

[4] Salih, S.J., & Mahmood, W.M. (2023). Review on magnetic spinel ferrite (MFe2O4) nanoparticles: From synthesis to application. Heliyon, 9(6), e16601.

[5] Poole, C.P., & Owens, F.J. (2003). Introduction to Nanotechnology. Wiley-Interscience, pp. 145–150.

[6] Da Silva, F.G., Depeyrot, J., Campos, A.F., et al. (2019). Structural and magnetic properties of spinel ferrite nanoparticles. Journal of Nanoscience and Nanotechnology, 19(8), 4888–4902.

[7] Shkir, M., Ahmad, N., Alshahrani, T., Ahmad, Z. and AlFaify, S., 2024. Novel CdFe2O4 nanoparticles facile synthesis and their applications towards practical ammonia detection: an effect of annealing. Physica Scripta, 99(10), p.105952.

[8] Devmunde, B.H., Bhalerao, P.S. and Solunke, M.B., 2020, October. Structural morphological and infrared properties of Cd2+ substitutes nickel ferrite particles. In Journal of Physics: Conference Series (Vol. 1644, No. 1, p. 012021). IOP Publishing.

[9] Rivani, D.A., Retnosari, I., Kusumandari, & Saraswati, T.E. (2019). Influence of TiO2 addition on the magnetic properties of carbon-based iron oxide nanocomposites. IOP Conf. Series: Mater. Sci. Eng., 509(1), 012034

[10] Sardar, I., Hossain, M.D., Sikder, M.S., Khan, M.N.I., & Rahman, M.R. (2024). Enhancement of coercivity, permeability, and dielectric properties of Co0.2Zn0.3Ni0.5EuxFe2−xO4 ferrites. Journal of Rare Earths, 42(6), 1128–1135.

[11] Tiwari, R., De, M., Tewari, H.S. and Ghoshal, S.K., 2020. Structural and magnetic properties of tailored NiFe2O4 nanostructures synthesized using auto-combustion method. *Results in Physics*, *16*, p.102916.

[12] Murthy, P.K., Kiran, K.S. and Melagiriyappa, E., 2024. Influence of Nd3+ on structural, electrical and magnetic properties of Ni-Cd nanoferrites. *Physics Open*, *21*, p.100240.

[13] Pathare, R.N., Daf, S.R., Chaudhari, Y.D., Anwane, S.W., Zingare, P.A. and Suryawanshi, S.M., 2026. Rare-Earth Doping in CdFe2O4 Spinel Ferrites: A Comprehensive Study of Structural, Elastic, Vibrational and Magnetic Properties. *Micro and Nanostructures*, p.208802.

[14] Rajenimbalkar, R.S., Deshmukh, V.J., Patankar, K.K. and Somvanshi, S.B., 2024. Effect of multivalent ion doping on magnetic, electrical, and dielectric properties of nickel ferrite nanoparticles. *Scientific Reports*, *14*(1), p.29547.

[15] Satish, M., Shashanka, H.M. and Anantharamaiah, P.N., 2023. Unravelling the role of zirconium-substitution on the magnetic properties of nickel ferrite processed from nanocrystalline powders. *Materials Today: Proceedings*, *89*, pp.95-99.

[16] El-Shater, R.E., El Shimy, H. and Assar, S.T., 2020. Investigation of physical properties of synthesized Zr doped Ni–Zn ferrites. *Materials Chemistry and Physics*, *247*, p.122758.

[17] Wanjari, S.S., Nandanwar, D.V., Rewatkar, K.G., Gongal, A.V. and Sarve, S.R., 2025. Structural and microwave absorption properties of Ni-doped Cd-La nanoferrites synthesized via sol-gel auto combustion route. *Ceramics International*.

[18] Nazli, H., Ahtasham, F., Razi, A. and Kayani, Z.N., 2025. In-situ oxidation time dependent low-cost synthesis of cadmium iron oxide thin films for electronic and spintronic devices. *Materials Research Bulletin*, p.113765.

[19] Singh, C.J., Choudhari, Y.D., Borikar, M.A., Kumhar, R.P., Sahu, D.K., Rewatkar, K.G., Daf, S.R. and Wazalwar, A.N., 2025. Microwave Assisted Sol-Gel Synthesis and Characterization of CoZr doped Zinc Spinel Ferrite: Structural, Magnetic and Electrical Properties. *Inorganic Chemistry Communications*, *180*, p.114977.

[20] Keerthana, S.P., Yuvakkumar, R., Ravi, G., Arunmetha, S., Thambidurai, M. and Velauthapillai, D., 2024. Magnetically separable rare earth metal incorporated CdFe2O4 photocatalyst for degradation of cationic and azo dyes. *Journal of Molecular Structure*, *1302*, p.137479.

[21] Nandanwar, A.K., Sarkar, N.N., Sahu, D.K., Choudhary, D.S. and Rewatkar, K.G., 2018. Effect of Ni+ 2 substitution on structural and electrical behaviour of nano-size cadmium ferrites. *Materials Today: Proceedings*, *5*(10), pp.22669-22674.

[22] Harish, K.N., BS, S., B, U., Pai, P.G., M, J.N., Khasim, S. and Reddy, S., 2026. An effective sensing platform of graphite-based Zr-CdFe2O4 nanoparticle for

electrochemical sensing of heavy metal Pb2+ ions and Sunlight-induced photo-degradation activity. *Journal of Materials Science: Materials in Electronics*, *37*(3), p.262.

[23] Mohammed, N., Bagum, A., Khan, M.S. and Hossen, M.B., 2025. Structural with Rietveld analysis and enhancement of magnetic, magnetocaloric study of Al substituted Ni–Cd bulk spinel ferrites. *Applied Physics A*, *131*(3), p.216.

[24] Teber, A. and Sarac, M.F., 2023. Electrical, Magnetic, Microstructural, and Characteristic Properties of Zirconium-Substituted Co 0.5 Ni 0.5 Zr x Fe 2− x O 4 Spinel Ferrite Nanostructures. *Arabian Journal for Science and Engineering*, *48*(6), pp.8153-8164.

[25] Langade, K.J., Patil, P.G. and Vyawahare, S.K., 2025. Cr^{3+} Substitution in Ni–Cd Ferrite Nanoparticles: Structural, Vibrational, and Magnetic Property Tuning via Sol–Gel Synthesis. *Journal of Inorganic and Organometallic Polymers and Materials*, *35*(12), pp.10306-10319.

[26] Liu, Q., Lv, L., Zhou, J.P., et al. (2012). Influence of nickel-zinc ratio on microstructure, magnetic and dielectric properties of Ni(1−x)ZnxFe2O4 ferrites. J. Ceram. Process. Res., 13(2), 110–116.

[27] Kavitha, S., & Kurian, M. (2019). Effect of zirconium doping in the microstructure, magnetic and dielectric properties of cobalt ferrite nanoparticles. J. Alloys and Compounds, 799, 147–159.

[28] Wanjari, S.S., Nandanwar, D.V., Rewatkar, K.G., & Gongal, A.V. (2024). Investigating impact of Ni-Cd substitution on structural magnetic and optical properties of nanosize Al ferrites. Heliyon (Elsevier), 10(21), e39734

[29] Wanjari, S.S., Nandanwar, D.V., Rewatkar, K.G., & Gongal, A.V. (2025). Unravelling the transformations: Comparative study of structural, magnetism, morphology, optical and microwave absorption properties in NiFe2O4 and CdFe2O4 spinel nanoparticles. Nano-Structures & Nano-Objects (Elsevier), 43, 101540. DOI: 10.1016/j.nanoso.2025.101540

[30] Ahamad, H.S., Meshram, N.S., Bankar, S.B., Dhoble, S.J., & Rewatkar, K.G. (2017). Structural properties of CuxNi1-xFe2O4 nano ferrites prepared by urea-gel microwave auto combustion method. Ferroelectrics, 516(1), 67–73. DOI: 10.1080/00150193.2017.1362285

[31] Vedrtnam, A., Kalauni, K., Dubey, S., & Kumar, A. (2020). A comprehensive study on structure, properties, synthesis and characterization of ferrites. AIMS Materials Science, 7(6), 800–835.

[32] Kumari, N., Kour, S., Singh, G., & Sharma, R.K. (2020). A brief review on synthesis, properties and applications of ferrites. AIP Conference Proceedings, 2220(1), 020164.

[33] Tolani, S.C., Golhar, A.R., & Rewatkar, K.G. (2019). A review of morphological, structural behaviour and technological applications of ferrites. AIP Conference Proceedings, 2104(1), 030032.

[34] Siddeshwar, M., Naveen, P. and Srinivas, K., 2024. Effect of Zr, Sm and Gd doped CoFe2O4 on structural, spectral and magnetic properties. *ECS Journal of Solid State Science and Technology*, *13*(8), p.083001.

[35] Banaj, L. and Agrawal, S., 2023. Dielectric behavior of Zr4+ doped MgFe2O4 spinel ferrite synthesized by solid-state reaction method. *Current Applied Physics*, *56*, pp.47-65.

[36] Thi, M.N.P., Diep, P.Q.T., Vuong, M.H.T., Nguyen, L.T., Nguyen, V.Y. and Nguyen, A.T., 2025. Structural distortion, optical band gap narrowing, and magnetic softening in Dy3+ _substituted NiFe2O4 nanoparticles synthesized via a simple co-precipitation route. Ceramics International.

[37] Li, F., Liu, J., Evans, D.G., & Duan, X. (2004). Stoichiometric synthesis of pure MFe2O4 spinel ferrites. Chemistry of Materials, 16(8), 1597–1602.

[38] Janbandhu, K.S. and Pawade, V.B., 2025. Structural and Optical Properties of NIR Laser Excited Ho3+/Yb3+ Doped Sr2LaF7 UC Phosphor. *Luminescence*, *40*(8), p.e70290.

[39] Kashid, P., Mathad, S.N., Shedam, M.R., et al. (2024). Facile fabrication and grain-size dependent structural behavior of Cadmium-Substituted nano Co-Ni ferrites. Ain Shams Engineering Journal, 15(3), 102549.

[40] Kharat, P.B., Chavan, A.R., Humbe, A.V., & Jadhav, K.M. (2019). Evaluation of thermoacoustics parameters of CoFe2O4–ethylene glycol nanofluid. J. Mater. Sci.: Mater. Electron., 30(2), 1175–1186.

[41] Zubair, A., Ahmad, Z., Mahmood, A., et al. (2017). Structural, morphological and magnetic properties of Eu-doped CoFe2O4 nanoferrites. Results in Physics, 7, 3203–3208.

[42] Sattibabu, B., Durga Rao, T., Das, T., et al. (2020). Synthesis and magnetic properties of nanostructured Ni1−xZnxFe2O4. AIP Conference Proceedings, 2269(1), 030076.

[43] Anwar, A., Zulfiqar, S., Yousuf, M.A., et al. (2020). Impact of rare earth Dy3+ cations on the various parameters of nanocrystalline nickel spinel ferrite. J. Mater. Res. and Technology, 9(3), 5313–5325.

[44] Qamar, S., Akhtar, M.N., Batoo, K.M., & Raslan, E.H. (2020). Structural and magnetic features of Ce doped Co-Cu-Zn spinel nanoferrites. Ceramics International, 46(10), 14481–14487.

[45] Islam, M.R., Rahman, M.M., & Hossain, A.K.M.A. (2023). Structural and magnetic properties of Ni–Cu–Zn spinel ferrite nanoparticles. J. Alloys and Compounds, 935, 167981.

[46] Kumar, S., Gupta, R., & Rani, R. (2022). Microwave-assisted synthesis of Cd-substituted cobalt ferrite nanoparticles. Materials Today: Proceedings, 62, 3415–3420.